

# Indirect Current Control of a Unity Power Factor Sinusoidal Current Boost Type Three-Phase Rectifier

JUAN W. DIXON AND BOON-TECK OOI, SENIOR MEMBER, IEEE

**Abstract**—The indirect current control scheme has evolved from the success of the hysteresis current controlled voltage regulated rectifier, which has been shown to be capable of: 1) unity and even leading power factor operation, 2) near sinusoidal current waveforms, and 3) bilateral power transfer without the need of bi-directional solid state power switches. The advance consists of replacing the inner hysteresis current feedback loop by the standard sinusoidal PWM control and in the process saving the cost of the current measuring transducers. The scheme is evaluated through tests on 1-KW size laboratory models and through digital simulations. A theory of the system dynamics is developed and stability boundaries are presented.

## INTRODUCTION

THE SUCCESSFUL application of the PWM techniques on the inverter side of the dc link has prompted recent investigations as to whether they have a more fitting role to play in replacing the conventional thyristor bridge rectifiers, which are notorious for harmonic pollution and poor power factor. The research is divided into adherents of the buck principle [1]–[4] and the boost principle [5]–[8]. The buck and boost principles are concepts developed in dc-to-dc switch-mode power supply design [9] and they have applicability in ac-to-dc conversion also.

The hysteresis current control rectifiers reported by the authors in several publications [5]–[8] fall under the boost principle. The pioneering works of hysteresis current control in inverter drives are listed in [10], [11].

The indirect current control reported here has evolved from a mature understanding of the previous research. As the name implies, the function of the inner hysteresis current control feedback loop is mimicked mathematically and implemented by hardware representing transfer function blocks. The ac currents are indirectly controlled by the standard sinusoidal PWM, which essentially modulates the fundamental harmonic component of the voltage. In eliminating the inner hysteresis current feedback loop, one dispenses with the need for at least two high-quality broad bandwidth current measuring transducers. But is there serious performance deterioration for which the cost savings are not justified?

Manuscript received August 19, 1987; revised March 29, 1988. This work was supported by the Natural Science and Engineering Research Council of Canada and the Ministry of Education, Quebec, through an FCAR grant. J. W. Dixon was supported in his postgraduate studies by the Catholic University of Chile.

The authors are with the Department of Electrical Engineering, McGill University, Montreal, P.Q. Canada, H3A 2A7.  
IEEE Log Number 8823352.

In partial answer to this question, this paper presents: 1) experimental test results from 1-KW size laboratory models, 2) studies from digital simulation, and 3) mathematical analysis of system dynamics. The paper is organized in three parts.

*Part I* briefly recapitulates the essential features of the boost rectifier and in particular the hysteresis current controlled rectifier. This serves the purposes of: 1) showing the thought process leading to the indirect current control and 2) laying the groundwork for making comparisons of the two systems.

*Part II* describes the principle of operation of the indirect current control and reports on its performance characteristics.

*Part III* presents the mathematical analysis of the system dynamics.

## I. BOOST TYPE BRIDGE RECTIFIER

Fig. 1 shows the schematic diagram of the hysteresis current controlled rectifier. The distinguishing features making it a *boost type* rectifier are: 1) the directions of the current flow through the power transistors and the antiparallel diodes, 2) the placement of the inductances  $L$  on the ac side, and 3) the placement of the capacitance  $C$  on the dc link side.

### A. Hysteresis Current Control

Fig. 1 shows the implementation of the inner current feedback loop of the  $a$ -phase. It is essentially a control that tracks a current reference. The current reference is derived from a waveform template. In this particular paper, the template waveform is taken from the voltage transformer across the phase voltage of the supply. The sinusoidal waveform is then phase shifted so that one can request unity or leading power factor operation. Since the hysteresis current control has been described previously, the details can be found in [10]–[12].

### B. Voltage Regulation—Proportional Feedback Loop

Neglecting losses in the rectifier, the power output of the rectifier  $i_1 v_c$  is equal to the ac power less the losses in the phase resistance  $R$  and the power going in  $L$  as storage magnetic energy. Hence the local average current  $i_1$  is obtained from the formula

$$i_1 = \frac{3 \left[ VI \cos \varphi - RI^2 - \frac{d}{dt} \frac{1}{2} LI^2 \right]}{v_c} \quad (1)$$

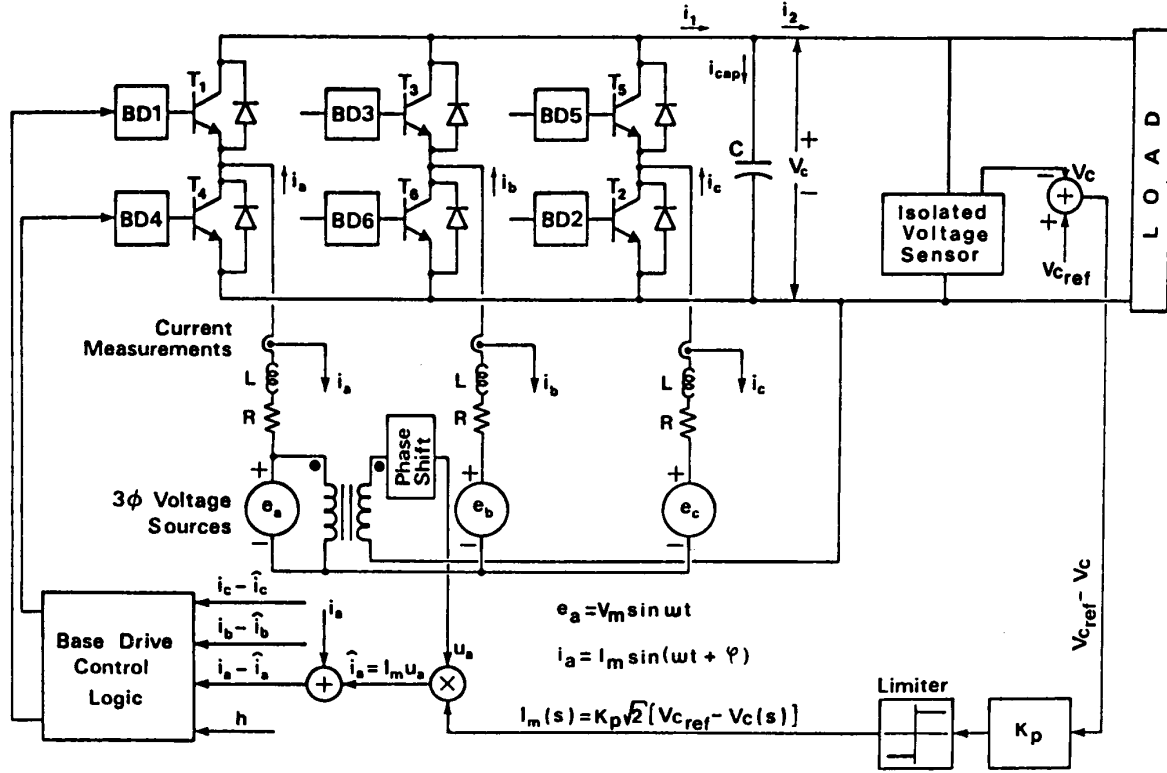


Fig. 1. Schematic diagram of hysteresis current controlled rectifier.

where  $v_c$  is the dc link voltage,  $V$  and  $I$  are the rms values of the phase supply voltage and current, respectively.

If the load current is  $i_2$ , then the dc link capacitance charging current based on Kirchoff's Current Law is

$$C \frac{dv_c}{dt} = i_1 - i_2. \quad (2)$$

For power matching,  $i_1$  must track the load current  $i_2$ . This is accomplished by an outer proportional feedback control loop that compares  $v_c$  with a set voltage reference  $V_{ref}$  and uses the error to control the current magnitude, i.e.

$$I = K_p (V_{ref} - v_c) \quad (3)$$

where  $K_p = \text{transfer gain } A/V$ .

## II. INDIRECT CURRENT CONTROL

### A. The Challenge

The challenge in engineering is to find ways of lowering cost by reducing component count. The indirect current control is proposed here to eliminate the inner hysteresis current controlled feedback loop and in so doing save the cost of two high-quality broad-band current transducers required for current measurements.

The method falls back on the well-known sinusoidal PWM control in which the switching instants are determined by the intersections of the triangular wave carrier and the modulating sine wave.

### B. Principle of Indirect Current Control

The objective is to be able to operate the rectifier so that the fundamental harmonic component of the phase current, which is represented by the phasor  $\vec{I}$  in Fig. 2, makes a constant power angle  $\varphi$ . As the rectifier becomes more heavily loaded, it is the current magnitude  $I$  that increases. For inverter operation  $I$  takes a negative value ( $180^\circ$  phase reversal).

Considering the fundamental harmonic of the supply frequency only, if the phase circuit impedance is  $\vec{Z} = R + j\omega L = R + jX$ , one can indirectly control the current by the fundamental component of the voltage  $\vec{V}_{ph}$  at the terminals of the rectifier. Based on Kirchoff's Voltage Law, the required voltage  $\vec{V}_{ph}$  is obtained from the equation

$$\vec{V}_{ph} = \vec{V} - \vec{I}\vec{Z}. \quad (4)$$

Equation (4) is represented in the phasor diagram of Fig. 2. In the time-domain, one sees that if

$$v_a(t) = \sqrt{2} V \sin \omega t \quad (5)$$

then the requisite control voltage has to be

$$v_{pha}(t) = \sqrt{2} V_{ph} [\cos \xi \sin \omega t - \sin \xi \cos \omega t] \quad (6)$$

where the in-phase component is

$$V_{ph} \cos \xi = V + (X \sin \varphi - R \cos \varphi) \cdot I \quad (7)$$

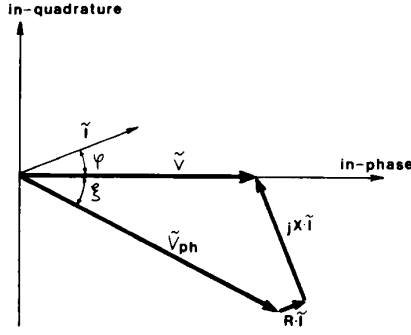
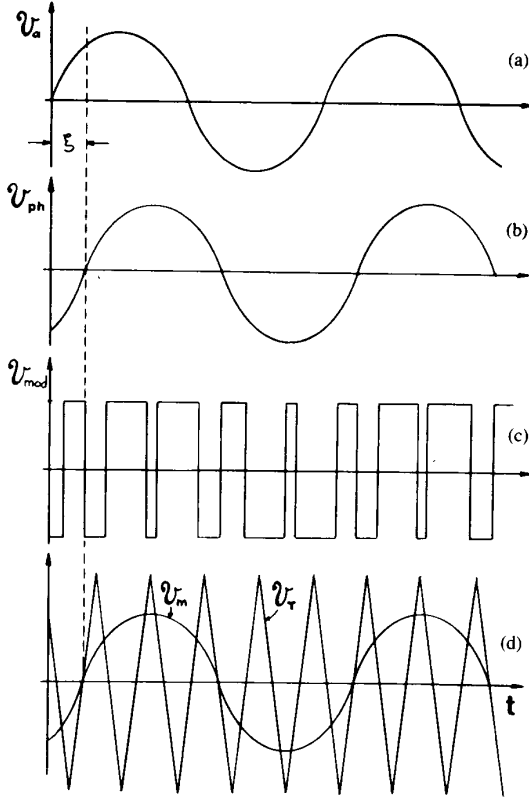


Fig. 2. Voltage phasor diagram of ac phase circuit.

Fig. 3. Waveforms of: (a)  $v_a(t)$ ,  $a$ -phase supply voltage, (b)  $v_{ph}(t)$ , fundamental component of phase voltage at  $a$ -phase rectifier terminal, (c)  $v_{mod}(t)$  switched voltage of which (b) is the fundamental, (d)  $v_T$  carrier and  $v_m(t)$  modulating waveform.

and the in-quadature component is

$$V_{ph} \sin \xi = (X \cos \varphi + R \sin \varphi) \cdot I. \quad (8)$$

From (7) and (8) one sees that since  $V$ ,  $R$ , and  $X$  can be measured beforehand from the ac circuit, one can operate at any power angle  $\varphi$  for any demand of the current magnitude  $I$  provided the in-phase and the quadrature components of  $\tilde{V}_{ph}$  are made to satisfy (7) and (8).

### C. Sinusoidal PWM Control

Fig. 3(a) and (b) illustrates the waveforms of  $v_a(t)$  and  $v_{ph}(t)$  of (5) and (6).

The voltage  $v_{ph}(t)$  is the fundamental component of the voltage at the rectifier terminals, the rectifier being under sinusoidal PWM control. If one imagines the capacitor  $C$  to have a center-tap, then the waveform of the voltage between the  $A$ -phase rectifier terminal and the center-tap consists of the square wave shown in Fig. 3(c). This modulating waveform switches from  $+0.5v_c$  to  $-0.5v_c$  and it is desired that the switching pattern is such that it yields as fundamental component the waveform of  $v_{ph}(t)$ .

Fig. 3(d) illustrates how the switching pattern is generated in the conventional sinusoidal PWM strategy. As described in the standard textbooks, the switching instants are based on the intersections of the triangular waveform  $v_T$  and the modulating sinusoidal waveform  $v_m(t)$ .

### D. Fourier Series of Sinusoidal PWM

The Fourier Series of the output voltage waveform is quite involved. Based on the formula given in [13], when the modulating signal is

$$v_m(t) = \sqrt{2} V_m [\cos \xi \sin \omega t - \sin \xi \cos \omega t] \quad (9)$$

the output voltage is

$$v_{mod}(t) = \frac{\sqrt{2}}{2} \frac{V_m}{V_{T\text{PEAK}}} v_c [\cos \xi \sin \omega t - \sin \xi \cos \omega t] \\ + \text{Bessel function harmonic terms} \quad (10)$$

for

$$V_m < V_{T\text{PEAK}} (\text{peak value of } v_T). \quad (11)$$

By increasing the carrier frequency, the fundamental component in (10) dominates over the harmonic terms, and consequently the harmonic distortion in the current can be made negligible.

### E. Modulating Signal $\tilde{V}_m$

The generation of the modulating signal of the  $A$ -phase is illustrated in the block diagram of Fig. 4. The input comes from the current magnitude demand  $I$ , which is based on the voltage error of the dc link voltage  $v_c$  with respect to the voltage reference  $V_{ref}$  as described in (3). This signal is combined with proportional amplifiers of gains  $K_1$ ,  $K_2$ , and  $K_3$ , multipliers, and the generators of the in-phase and the in-quadature waveforms. The intent is to produce the modulating signal  $v_m(t)$  in (9), which will result in the fundamental component in (10) being identical to (6).

The in-phase waveform generator is taken from the voltage transformer across the line-to-neutral of the  $A$ -phase. After filtering its output is

$$v_x = \sqrt{2} V_s \sin \omega t. \quad (12)$$

The in-quadature waveform generator is obtained from subtracting the  $B$ -phase from the  $C$ -phase voltage, and multiplied by  $1/\sqrt{3}$  factor so that its output is

$$v_y = \sqrt{2} V_s \cos \omega t. \quad (13)$$

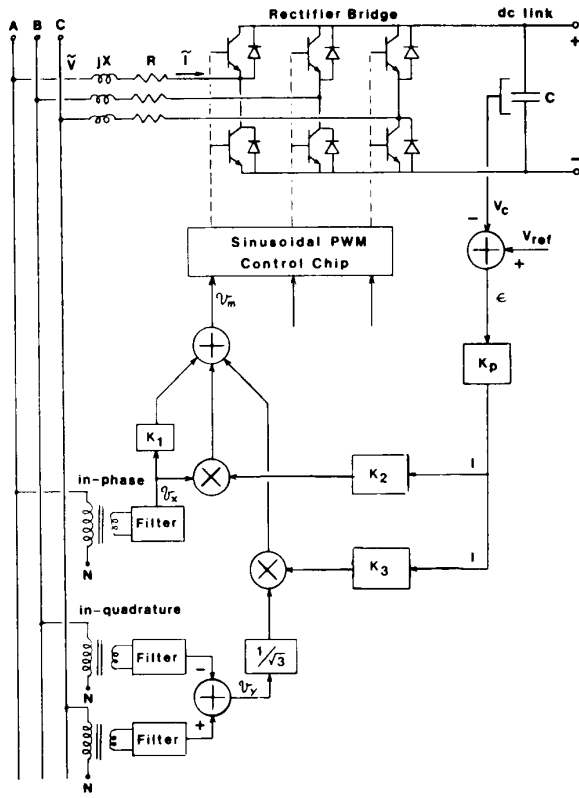


Fig. 4. Block diagram implementing indirect current control.

For the  $v_m(t)$  prescribed by the functional blocks of Fig. 4, the output voltage at the rectifier terminal is

$$v_{\text{mod}}(t) = \frac{\sqrt{2}}{2} \frac{V_s}{V_{T \text{ PEAK}}} v_c [(K_1 + K_2 I) \sin \omega t - K_3 I \cos \omega t] + \text{Bessel function harmonic terms.} \quad (14)$$

The objective is to make the fundamental component in (14) identical to (6)–(8). This is done by choosing the values of the constants  $K_1$ ,  $K_2$ , and  $K_3$ . But before doing that, one needs to compensate for the voltage droop.

**F. Voltage Droop Compensation**

One notices in (14) that the magnitude of the fundamental voltage in (14) is proportional to  $v_c$ . The proportional feedback of the voltage regulated feedback loop has an inherent voltage droop. In order to correct it, the output of the triangular carrier generator is multiplied by voltage  $v_c$  so that

$$V_{T \text{ PEAK}} = K_4 v_c. \quad (15)$$

**G. Choosing Constants  $K_1$ ,  $K_2$ , and  $K_3$**

By comparing (14) with (6)–(8), the amplifier gains  $K_1$ ,  $K_2$ , and  $K_3$  are determined as

$$K_1 = 2K_4 V_A / V_s \quad (16)$$

$$K_2 = 2K_4 \frac{(X \sin \varphi - R \cos \varphi)}{V_s} \quad (17)$$

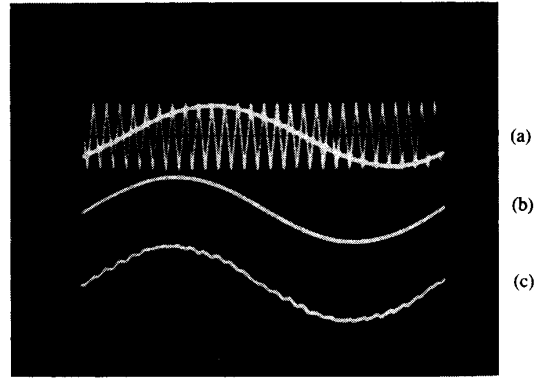


Fig. 5. Unity power factor operation. (a) Modulating signal  $v_m$  and carrier  $v_T$ . (b) Supply voltage  $v_A$ . (c) Rectifier input current  $v_A$ .

$$K_3 = 2K_4 \frac{(X \cos \varphi + R \sin \varphi)}{V_s} \quad (18)$$

**H. Experimental Test Results**

Implementation on a 1-KW bipolar transistor experimental unit shows very good performance characteristics. Fig. 5 is a record of steady-state, unity power factor operation as a rectifier. Of particular interest is the phase relationship of the modulating signal in Fig. 5(a) with respect to the supply voltage in Fig. 5(b) to maintain the current in Fig. 5(c) at unity power factor.

Fig. 6 is a record of a power reversal experiment from  $-7A$  dc (inversion) to  $5A$  dc (rectification).

Using the waveform of the phase voltage of Fig. 6(c) as a reference, one sees that in passing from inversion to rectification the current waveform of Fig. 6(d) has a  $180^\circ$  phase reversal. One sees in Fig. 6(b) that the modulating waveform  $v_m$  has a large magnitude and leads  $v_A$  in inverter operation and has a lower magnitude and lags  $v_A$  in the rectifier operation. Since  $V_m$  is essentially controlling  $\vec{V}_{ph}$ , one has only to return to the phasor diagram of Fig. 2 to be convinced that  $\vec{V}_{ph}$  has a large magnitude and leads the  $\vec{V}$  when the current direction is reversed from inverter operation.

**I. Reliability of Digital Simulation Program**

The experimental work has been pursued together with digital simulation studies. The valve-by-valve digital simulation program is based on treating the rectifier bridge of Fig. 4 as a piece-wise circuit problem. The ON-OFF states of each of the six power-transistors give rise to eight possible circuit topologies. The instants of switchings of the transistors are monitored by keeping track of the intersections of the triangular carrier and the modulating signal of each phase and thus a time sequence of the eight circuit topologies is generated. The differential equations arising from the Kirchhoff Voltage and Current Laws for the topologies are solved numerically and they are joined together by the requirements that the flux linkages and electric charges must be continuous.

Comparisons of several digital simulation predictions with experimental measurements, of which Figs. 6 and 7 are examples, show that one can rely on the simulation program as being correct.

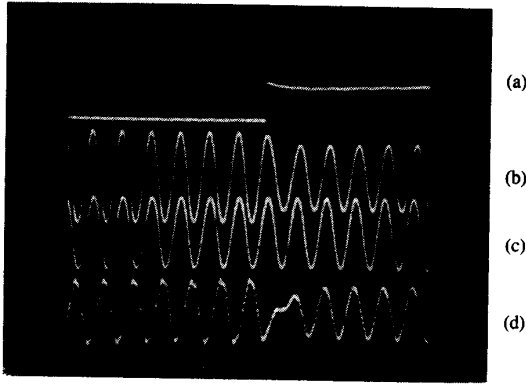


Fig. 6. Step reversal power. (a)  $i_2$ , from  $-7$  to  $5A$  dc. (b)  $v_m$ . (c)  $v_a$ . (d)  $i_a$ .

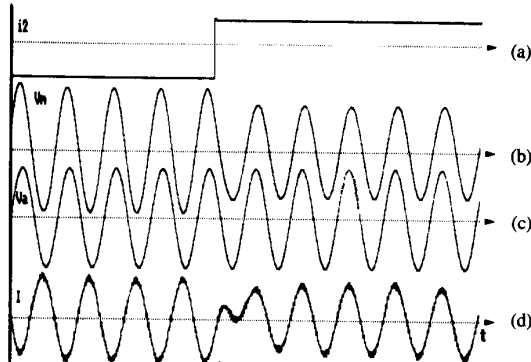


Fig. 7. Valve-by-valve digital simulation of experimental measurements of Fig. 6.

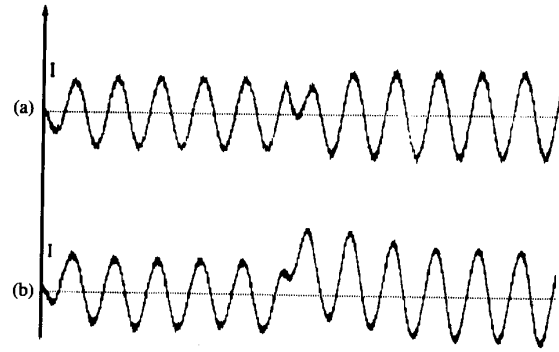
#### J. Comparison of Hysteresis Current Control with Indirect Current Control

Fig. 8 compares the hysteresis current control with the indirect current control in a step reversal of power from inverter operation to rectifier operation. The results are obtained from the Valve-by-Valve Digital Simulation Program.

The hysteresis current control has a better response characteristic as the sinusoidal waveform is restored after a brief transient. In contrast, the indirect current control can give rise to a dc offset as is the case in Fig. 8. This dc offset is familiar in the study of ac transients in highly inductive circuit. As is made clear in Part III, it arises because the voltage  $\bar{V}_{ph}$  is controlling the phase current. The dc offset does not appear in the hysteresis current control because the inner feedback loop ensures that the current template waveforms are tracked closely at all times.

### III. ANALYSIS OF SYSTEM DYNAMICS

The analytical study is pursued to answer the fundamental question as to how the indirect current controller should be modeled mathematically. The correct analytical model should be able to predict the stability limits that are found in inverter operation in addition to the limits in rectifier operation. In hysteresis current control, instability is found in rectifier operation only.



$i_2$ : from  $-6$  to  $6$  A  $V_a = 40$  V  $V_c = 120$  V  $L = .0065$  H  $R = .75$  Ohm  $C = 12$  nF  
Fig. 8. Valve-by-valve digital simulation of a step reversal of power. (a) Hysteresis current control. (b) Indirect current control.

#### A. Instantaneous Response in Sinusoidal PWM Controller

Referring to Fig. 4, one sees that the input signal  $I$  is electronically multiplied to the in-phase and the in-quadrature waveforms so that  $(K_1 + K_2I)$  and  $-K_3I$  appear as the coefficients of  $\sin \omega t$  and  $\cos \omega t$  in (14). The point to make is that there is no time delay at this stage and  $\bar{V}_{ph}$  responds instantaneously to  $I$ .

Time delays are therefore due to the energy storage elements  $L$  and  $C$ .

#### B. Unity Power Factor Controller

It is assumed that all time harmonic terms are negligible. For simplicity, the analysis is based on a unity power factor controller. For a supply phase voltage

$$v_a = \sqrt{2} V \sin \omega t. \quad (19)$$

From (6)–(8) for the case  $\varphi = 0$ , it is required that

$$v_{pha}(t) = \sqrt{2} [(V - IR) \sin \omega t - IX \cos \omega t]. \quad (20)$$

The phase current is solved from the differential equation based on Kirchhoff's Voltage Law.

$$L \frac{d}{dt} i_a + R i_a = v_a(t) - v_{pha}(t). \quad (21)$$

For a constant value of  $I$ , in (20) the steady-state solution of (21) is

$$i_{ass} = \sqrt{2} I \sin \omega t. \quad (22)$$

The transient solution of (21) is

$$i_{at} = A \exp(-t/T) \quad (23)$$

where  $A$  is the constant of integration and  $T = L/R$  and

$$i_a = \sqrt{2} I \sin \omega t + A \exp(-t/T). \quad (24)$$

The off-set current problem is essentially the recognition of the transient component of (23).

In general,  $I$  is not a constant but is a time function  $I(t)$  determined from the simultaneous solution of (2) and (3).

There is a set of (19)–(24) for the  $b$ -phase and for the  $c$ -phase with the time delay angles of  $120^\circ$  and  $240^\circ$ , respectively.

### C. Dynamic Power Balance Equation

The ac power entering the terminals of the rectifier is

$$P_{ac} = v_{pha}(t)i_a(t) + v_{phb}(t)i_b(t) + v_{phc}(t)i_c(t). \quad (25)$$

If  $i_1$  is the local average of the output current of the rectifier dc terminal, the dc power output is

$$P_{dc} = i_1 v_c. \quad (26)$$

Assume negligible losses in the rectifier

$$P_{dc} = P_{ac} \quad (27)$$

### D. Capacitive Power Input

Multiplying (2) by  $v_c$ , one has

$$v_c C \frac{dv_c}{dt} = P_{dc} - P_{load}. \quad (28)$$

Substituting (25) into (27) and thereafter (27) into (28)

$$\frac{dv_c}{dt} = \frac{v_{pha}(t)i_a(t) + v_{phb}(t)i_b(t) + v_{phc}(t)i_c(t) - P_{load}}{Cv_c} \quad (29)$$

### E. Justification of Analytical Model

There are four ordinary differential equations describing the dynamics of the indirect current controlled rectifier. Three of these consist of the  $a$ ,  $b$ , and  $c$  phases of (21). The  $b$  and  $c$  phases enter into the right-hand side of (21) as phase angle shifts of  $-120^\circ$  and  $-240^\circ$  in (19) and (20).

The fourth differential equation is in (29).

The algebraic equation of (3) describes the proportional control of the voltage feedback loop.

In the case where the three-phase power supply is  $Y$ -connected without a neutral return (as is assumed in this study), the algebraic equation

$$i_a + i_b + i_c = 0 \quad (30)$$

allows the system equations to be reduced from 4th order to 3rd order.

A series of tests have shown that the predictions from the analytical model are in very good agreement with those predicted from the detailed model of the rectifier based on the sequence of network topologies determined by ON-OFF switching instants of the power transistors (valve-by-valve switching model). The tests have included situations: 1) where the rectifier is on the margin of instability and 2) where the rectifier in fact becomes unstable.

### F. Stability Analysis

With confidence in the correctness of the analytical model, the next stage is to proceed toward making it as a tool for

stability analysis. As (29) is nonlinear, the standard technique is to perturb about the equilibrium point  $\bar{x} = \bar{x}_0 + \Delta x$  to obtain

$$\frac{d}{dt} \Delta x = [A] \Delta x. \quad (31)$$

If  $[A]$  is a constant matrix, then the system is stable if none of its eigenvalues appear on the right-hand-side of the  $s$ -plane.

The immediate difficulty is that since the phase voltages

$$v_{abc} = \begin{bmatrix} v_a \\ v_b \\ v_c \end{bmatrix} = \sqrt{2} V \begin{bmatrix} \sin \omega t \\ \sin(\omega t - 120^\circ) \\ \sin(\omega t - 240^\circ) \end{bmatrix} \quad (32)$$

are time dependent, the equilibrium operating point  $\bar{X}_0(t)$  is also time dependent and so will  $[A]$  be in (31).

This slight embarrassment is overcome by using the well-known power invariant transformations [14]

$$v_{0\alpha\beta} = [C_1] v_{abc} \quad (33)$$

$$\dot{i}_{0\alpha\beta} = [C_1] \dot{i}_{abc} \quad (34)$$

where

$$[C_1] = \sqrt{\frac{2}{3}} \begin{bmatrix} \frac{\sqrt{2}}{2} & \frac{\sqrt{2}}{2} & \frac{\sqrt{2}}{2} \\ 1 & -\frac{1}{2} & -\frac{1}{2} \\ 0 & \frac{\sqrt{3}}{2} & -\frac{\sqrt{3}}{2} \end{bmatrix} \quad (35)$$

and then

$$v_{odq} = [C_2] v_{0\alpha\beta} \quad (36)$$

$$\dot{i}_{odq} = [C_2] \dot{i}_{0\alpha\beta} \quad (37)$$

where

$$[C_2] = \begin{bmatrix} 1 & 0 & 0 \\ 0 & \cos \omega t & \sin \omega t \\ 0 & -\sin \omega t & \cos \omega t \end{bmatrix} \quad (38)$$

Applying the transformations of (35) and (38) to the  $a$ ,  $b$ , and  $c$ -phases of (21) and assuming  $Y$ -connection without neutral of (30) so that the zero-sequence does not exist, one has

$$L \frac{di_d}{dt} + Ri_d - L\omega i_q = \sqrt{3} IX \quad (39)$$

$$L \frac{di_q}{dt} + Ri_q + L\omega i_d = -\sqrt{3} IR. \quad (40)$$

Equation (29) is transformed to

$$\frac{dv_c}{dt} = \frac{[-(V - IR)i_q - IXi_d] - P_{load}}{Cv_c} \quad (41)$$

### G. Equilibrium Operating Point

From (39) and (40), the steady-state solutions are

$$I_d = 0 \quad (42)$$

$$I_q = -\sqrt{3}I_0 \quad (43)$$

where  $I_0$  is solved from the quadratic equation obtained by equating (41) to zero.

$$P_{\text{load}} = 3[VI_0 - I_0^2 R]. \quad (44)$$

From (3)

$$V_c = V_{\text{ref}} - \frac{I_0}{K_p}. \quad (45)$$

### H. Characteristic [A]-matrix

Defining

$$\Delta X = \begin{bmatrix} \Delta V_c \\ \Delta i_d \\ \Delta i_q \end{bmatrix} = \begin{bmatrix} v_c - V_c \\ i_d - I_d \\ i_q - I_q \end{bmatrix} \quad (46)$$

and applying small perturbation linearization of (39)–(41) one obtains (31) where

$$[A] = \begin{bmatrix} \frac{3K_p I_0 R}{CV_c} & -\frac{\sqrt{3}I_0 X}{CV_c} & -\frac{\sqrt{3}(V - I_0 R)}{CV_c} \\ -\frac{\sqrt{3}K_p X}{L} & -\frac{R}{L} & \omega \\ \sqrt{3}K_p \frac{R}{L} & -\omega & -\frac{R}{L} \end{bmatrix} \quad (47)$$

### I. Eigenvalue Analysis

The eigenvalues of the [A]-matrix of (47) are evaluated numerically by an IMSL subroutine [15]. Fig. 9 shows the stability boundaries of indirect current control for  $K_p = 3$ ,  $V_c = 120$ ,  $V = 40V$ ,  $L = 0.005H$ . The analytical predictions are verified by tests using the Valve-by-Valve Program. The hysteresis current control has superior stability characteristics as shown in Fig. 9.

One sees that instability becomes serious as the ac phase resistance  $R$  is reduced and there is good reason to believe that it is related to the increased time constant  $T = L/R$  in the ac circuit.

### J. Discussion

Since the indirect current control depends on the formation of  $v_m$  from the assigned values of  $K_1$ ,  $K_2$ , and  $K_3$  in Fig. 4, there is a concern that  $L$  must be big enough to accommodate any modeling errors. For instance, if  $\omega L = X$  varies from 0.02 to 0.03 p.u., say, then a 1-percent error in  $\vec{V}_{ph}$  can cause a 50–100 percent error in the current. Desensitizing can come from using large values of  $L$ , but this can be costly.

On analysis, it is found that this concern is unnecessary.

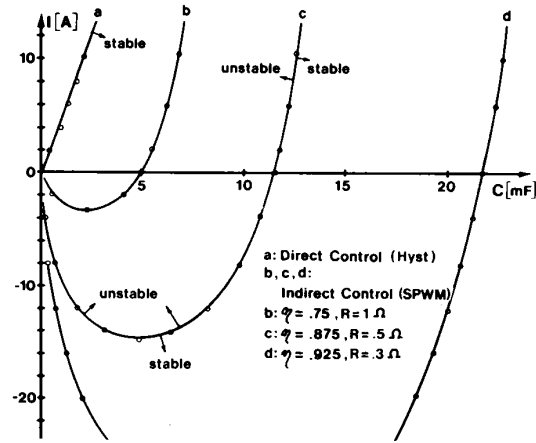


Fig. 9. Stability boundaries comparing indirect current control with hysteresis current control. Analytical predictions—lines. Valve-by-valve digital simulation—points.

This is because with the feedback loop, the current  $I$  is solved from the power balance equation

$$VI \cos \phi - RI^2 = P_{\text{load}}/3 \quad (48)$$

where

$$\cos \phi = \frac{RR_c + XX_c}{\sqrt{(R^2 + X^2)(R_c^2 + X_c^2)}} \quad (49)$$

and when  $R_c$  and  $X_c$  are the values used in (17) and (18) for  $K_2$  and  $K_3$ .

For a typical numerical example, it is found that a 50-percent difference between  $X$  and  $X_c$  causes only a 2-percent change in current. This is confirmed experimentally. In the laboratory, when  $X$  differed from  $X_c$  by 100 percent, the current change was not detectable in the instrumentation. From control theory, it is well known that the feedback loop renders the system relatively insensitive to component parameters.

### CONCLUSIONS

From experimental tests, the indirect current control scheme has been shown to be practical and promising. The study is limited to the case of a simple proportional voltage regulator feedback and in this instance the transient response and stability characteristics are inferior to those of the hysteresis current controlled scheme. However, there is an entire repertoire of feedback compensation methods and further study should be able to show that significant improvement can be realized.

Another important contribution of this paper consists of developing the analytical theory to the extent that transients and stability limits can be predicted accurately.

### ACKNOWLEDGMENT

The authors are indebted to J. Mui for laboratory assistance and S. Papineau for the preparation of the manuscript.

## REFERENCES

- [1] T. Kataoka, K. Mizumachi, and S. Miyairi, "A pulse width controlled AC-to-DC converter to improve power factor and waveform of AC line," *IEEE Trans. Ind. Appl.*, vol. IA-15, no. 6, pp. 670-675, Nov./Dec. 1979.
- [2] L. Malesani and T. Paolo, "Three phase AC/DC PWM converter with sinusoidal AC currents with minimum filter requirements," *IEEE Trans. Ind. Appl.*, vol. IA-23, no. 1, pp. 71-77, Jan./Feb. 1987.
- [3] P. D. Ziogas, Y.-G. Kang, and V. R. Stefanovic, "PWM control techniques for filter minimization," *IEEE Trans. Ind. Appl.*, vol. IA-21, no. 5, pp. 1206-1214, Sept./Oct. 1985.
- [4] A. Busse and J. Holtz, "Multiloop control of a unity power factor fast switching AC to DC converter," in *Proc. Power Electronics Specialist Conf.*, pp. 171-179, 1982.
- [5] B. T. Ooi, J. W. Dixon, A. B. Kulkarni, and M. Nishimoto, "An integrated AC drive system using a controlled current PWM rectifier inverter link," in *Proc. Power Electronics Specialist Conf. (Vancouver)*, pp. 23-27, June 1986.
- [6] J. W. Dixon, A. B. Kulkarni, M. Nishimoto, and B. T. Ooi, "Characteristics of a controlled-current PWM rectifier-inverter link," in *Proc. IEEE Ind. Appl. Soc. Ann. Meeting (Denver)*, pp. 685-691, Oct. 1986.
- [7] M. Nishimoto, J. W. Dixon, A. B. Kulkarni, and B. T. Ooi, "An integrated controlled-current PWM rectifier-chopper link for sliding mode position control," in *Proc. IEEE Ind. Appl. Soc. Ann. Meeting (Denver)*, pp. 752-757, Oct. 1986.
- [8] X. Ma, "High-performance PWM frequency changes," *IEEE Trans. Ind. Appl.*, vol. IA-22, no. 2, pp. 267-280, Mar./April 1986.
- [9] P. R. K. Chetty, *Switch-Mode Power Supply Design*. TAB BOOKS Inc., 1986, p. 5.
- [10] J. F. Eastham, A. R. Daniels, and Lipczynski, "A novel power inverter configuration," presented at the IEEE Ind. Appl. Soc. Ann. Meeting, Cincinnati, OH, 1980.
- [11] S. C. Peak and A. B. Plunkett, "Transistorized PWM induction motor drive system," *IEEE Trans. Ind. Appl.*, vol. IA-19, pp. 379-387, May/June 1983.
- [12] B. T. Ooi, J. C. Salmon, J. W. Dixon, and A. B. Kulkarni, "A 3-phase controlled current PWM converter with leading power factor," *IEEE Trans. Ind. Appl.*, vol. IA-23, pp. 78-84, Jan./Feb. 1987.
- [13] B. K. Bose, *Power Electronics and AC Drives*. Englewood Cliffs, NJ: Prentice-Hall, 1986, pp. 140-152.
- [14] H. K. Messerle, *Dynamic Circuit Theory*. New York: Pergamon, 1965, pp. 462-463.
- [15] IMSL Library, Edition 7, EIGRF-eigenvalues of real matrix.